Collinear spin-density-wave ordering in Fe/Cr multilayers and wedges

R. S. Fishman
Solid State Division, Oak Ridge National Laboratory, Oak Ridge, Tennessee 37831-6032

Zhu-Pei Shi
Read-Rite Corporation, R & D Division, 345 Los Coches Street, Milpitas, California 95035
(Received 6 April 1998; revised manuscript received 5 February 1999)

Several recent experiments have detected a spin-density wave (SDW) within the Cr spacer of Fe/Cr multilayers and wedges. We use two simple models to predict the behavior of a collinear SDW within an Fe/Cr/Fe trilayer. Both models combine assumed boundary conditions at the Fe-Cr interfaces with the free energy of the Cr spacer. Depending on the temperature and the number N of Cr monolayers, the SDW may be either commensurate (C) or incommensurate (I) with the bcc Cr lattice. Model I assumes that the Fe-Cr interface is perfect and that the Fe-Cr interaction is antiferromagnetic. Consequently, the I SDW antinodes lie near the Fe-Cr interfaces. With increasing temperature, the Cr spacer undergoes a series of transitions between I SDW phases with different numbers n of nodes. If the I SDW has $n=m$ nodes at $T=0$, then n increases by one at each phase transition from m to $m-1$ to $m-2$ up to the C phase with $n=0$ above $T_{IC}(N)$. For a fixed temperature, the magnetic coupling across the Cr spacer undergoes a phase slip whenever n changes by one. In the limit $N\rightarrow\infty$, $T_{IC}(N)$ is independent of the Fe-Cr coupling strength. We find that $T_{IC}(\infty)$ is always larger than the bulk Néel transition temperature and increases with the strain on the Cr spacer. These results explain the very high IC transition temperature of about 600 K extrapolated from measurements on Fe/Cr/Fe wedges. Model II assumes that the I SDW nodes lie precisely at the Fe-Cr interfaces. This condition may be enforced by the interfacial roughness of sputtered Fe/Cr multilayers. As a result, the C phase is never stable and the transition temperature $T_N(N)$ takes on a seesaw pattern as $n\geqslant 2$ increases with thickness. In agreement with measurements on both sputtered and epitaxially grown multilayers, model II predicts the I phase to be unstable above the bulk Néel temperature. Model II also predicts that the I SDW may undergo a single phase transition from $n=m$ to $m-1$ before disappearing above $T_N(N)$. This behavior has recently been confirmed by neutron-scattering measurements on CrMn/Cr multilayers. While model I very successfully predicts the behavior of Fe/Cr/Fe wedges, a refined version of model II describes some properties of sputtered Fe/Cr multilayers. [S0163-1829(99)03021-0]

I. INTRODUCTION

The original discovery of giant magnetoresistance[1] in Fe/Cr multilayers inspired an intensive investigation into their magnetic and electrical properties. Although giant magnetoresistance was soon found in other multilayers with nonmagnetic spacers, Fe/Cr heterostructures have continued to hold the interest of the physics community. Due to the competition between the spin-density wave (SDW) ordering in the Cr spacer[2] and the Fe-Cr interactions at the interfaces, Fe/Cr multilayers and wedges provide new insights into the physics of transition-metal magnets.

In bulk Cr, commensurate (C) or incommensurate (I) SDW's are stabilized in different ranges of doping. For Fe/Cr multilayers, neutron-scattering measurements[3,4] reveal that the I phase is stable when the number of monolayers (ML's) N inside the Cr spacer is greater than 30 or when the temperature is lower than the Néel temperature 310 K of pure Cr. By contrast, scanning electron microscopy measurements[5] on Fe/Cr/Fe wedges indicate that the I phase is stable for $N>23$ ML and up to at least 550 K. As the thickness of the wedge increases, the Fe-Fe coupling alternates between ferromagnetic (F) and antiferromagnet (AF) with phase slips every 20 ML at room temperature. To explain these measurements, we have introduced two different models for the SDW within the Cr spacer. Both models combine assumed boundary conditions at the Fe-Cr interfaces with the free energy of the Cr spacer. Model I takes the interfaces to be perfect and the Fe-Cr interactions to be antiferromagnetic. Consequently, only collinear C and I phases are stable and the I SDW antinodes lie close to the interfaces. Model II takes the I SDW nodes to lie precisely at each Fe-Cr interface. This condition restricts the SDW wave vector to quantized values. As a result, the Néel temperature changes discontinuously whenever the number of I SDW nodes changes by one. While model I quite successfully describes the properties of Fe/Cr wedges, model II may partially describe the behavior of sputtered Fe/Cr multilayers.

Because SDW formation in bulk Cr relies on the balance between magnetoelastic and Coulomb energies,[6] the amplitude and wave vector of the SDW are notoriously sensitive to both doping and pressure.[2] The d bands of Mn and V contain one extra or one fewer electron than Cr. So Mn or V impurities are often used to control the level of the chemical potential and the wave vector of the SDW. Cooled below its Néel temperature of 310 K, pure Cr enters an I state with a node-to-node distance of 27 ML. When the Mn concentration exceeds 0.3%, $Cr_{1-x}Mn_x$ enters a C state with an enhanced Néel temperature. By contrast, doping with V makes the SDW more incommensurate and shortens the distance

between nodes. With 2% V impurities, the Néel temperature is reduced to about half that of pure Cr and the node-to-node distance at T_N is shortened to about 13 ML.

Remarkably, applying pressure to bulk Cr has the same effect as doping with V: the Néel temperature decreases and the SDW becomes more incommensurate. A volume compression of 1.5% corresponds to doping with about 1% V impurities.[7] Alternatively, a pressure of 2.8 GPa corresponds roughly to lowering the electron concentration by 1%.[8] Since Fe has a slightly smaller lattice constant than Cr, the lattice strain exerted on the Cr spacer in an Fe/Cr wedge should lower[9] the bulk Néel temperature T_N and make the SDW more incommensurate. Below T_N, model I implies that the distance between phase slips approaches the node-to-node distance for the bulk SDW as N increases. Hence, the measured distance between phase slips of 20 ML at room temperature confirms that the SDW of the Cr spacer in an Fe/Cr wedge is more incommensurate than in pure Cr.

Strain is far less significant in Fe/Cr multilayers. Low-temperature measurements by Fullerton *et al.*[4] reveal that the SDW period is about 59 Å , corresponding to a node-to-node distance of 20 ML. This is quite close to the period of pure Cr (Ref. 2) at low temperatures.

The difference between Fe/Cr multilayers and wedges raises an intriguing puzzle. Although the large strain in Fe/Cr wedges should reduce the Néel temperature of the Cr spacer far below its value in pure, unstrained Cr, the measured IC transition temperature of the wedge is at least 550 K, far higher than the transition temperature of relatively strain-free multilayers. But as shown in Sec. III for large N, the IC transition temperature T_{IC} of model I is independent of the size of the Fe-Cr coupling constant. Unlike the Néel temperature T_N of the bulk alloy, T_{IC} *increases* with V doping and with strain.

Because the distance between interfacial steps is much shorter in sputtered multilayers than in epitaxially grown multilayers, the behavior of the SDW in epitaxial and sputtered Fe/Cr multilayers is quite different. While experiments[10,11] on epitaxially grown trilayers report that the Fe-Cr interaction is antiferromagnetic, measurements by Fullerton *et al.*[4] on sputtered multilayers suggest that the SDW nodes lie close to the Fe-Cr interfaces. Consequently, the Cr spacer does not magnetically couple the neighboring Fe layers in a sputtered multilayer.

The precise nature of the IC transition is also in some doubt. In the sputtered mutlilayers studied by Fullerton *et al.*, a remnant C phase is observed at low temperatures below 30 ML but does not appear at higher thicknesses above T_N. But in the epitaxially grown multilayers studied by Schreyer *et al.*,[3] an I SDW coexists with a noncollinear, helical (H) SDW between 200 and 300 K. The reported H SDW is believed to couple neighboring Fe moments at 90° angles, with the Fe moments returning to the same orientation every other layer.[12] Recent work[13,14] indicates that a H SDW is produced by the well-separated interfacial steps of epitaxially grown multilayers.

Many of the unique features of sputtered Fe/Cr multilayers can be attibuted to either interfacial roughness or the intermixing of Fe within the first few ML's of the spacer. Both roughness and intermixing frustrate the antiferromagnetic Fe-Cr interaction.[13] An I SDW can avoid such frustration by placing a node at each interface. Assuming that a node is fixed at each interface, the SDW wave vector is obtained by minimizing the free energy with respect to the total number $n \geqslant 2$ of SDW nodes. This model is developed in Sec. IV.

Unfortunately, model II only partially describes the properties of sputtered multilayers. Of course, the C phase is never stabilized by this model because a C SDW has no nodes. In agreement with Fullerton *et al.*,[4] model II predicts that the paramagnetic (P) to I transition always occurs below the bulk Néel transition. As very recently observed in CrMn/Cr multilayers,[15] model II permits phase transitions between SDW's with different numbers of nodes. However, this model also predicts that the Néel temperature suddenly drops when n increases by 1. The resulting seesaw pattern for $T_N(N)$ is quite unlike the monotonically increasing Néel temperature observed in sputtered multilayers.[4] Even after the positions of the SDW nodes are allowed to shift a few ML's from each interface, the first large drop in the Néel temperature from $n=2$ to $n=3$ survives.

This paper is divided into five basic sections. A brief tutorial on the SDW in bulk Cr is presented in Sec. II. Sections III and IV develop models I and II, respectively, and present their results. A discussion and conclusion is given in Sec. V. We obtain the large N dependence of the magnetic coupling for model I in Appendix A. Also in the large N limit, the IC transition temperature of model I is derived in Appendix B. The basic ideas of this work were first presented in three short papers: Refs. 16 and 17 were devoted to model I while model II was first developed in Ref. 18.

II. SPIN-DENSITY WAVE AND FREE ENERGY OF BULK Cr

The SDW instability[19] in Cr alloys is produced by the Coulomb attraction U between electrons and holes on nearly perfectly nested[20,21] electron a and hole b Fermi surfaces, both roughly octahedral in shape.[22] The electron Fermi surface centered at Γ and the hole Fermi surface centered at the zone boundary H are separated by wave vector $\mathbf{G}/2$, where $\mathbf{G}$ is a reciprocal lattice vector with magnitude $4\pi/a$. Together with the electron pockets around the X points, the a Fermi surface forms part of the so-called ''electron jack.'' Also present are hole pockets at the N points. Both the electron and hole pockets play an ancillary role in the formation of the SDW and are often grouped together into an electron ''reservoir'' that supplies electrons to the a and b Fermi surfaces once the quasiparticle gap opens below T_N.

However, these pockets may directly affect the magnetic coupling across an Fe/Cr/Fe trilayer. As discussed in the next section, the periodicity of that magnetic coupling is determined by the extremal points of the Fermi surface.[23,24] For this reason, oscillatory coupling has also been observed in Fe/Cu and Fe/Ag multilayers,[23] where the Cu or Ag spacer is paramagnetic. Quasiparticle transitions across the necks of the electron jack[25] or, alternatively, across the hole pockets,[23] are associated with a long period oscillation of the magnetic coupling in Fe/Cr multilayers and wedges.

Because the electron Fermi surface is slightly smaller than the hole Fermi surface, there are two different nesting wave vectors $\mathbf{Q}_{\pm}$ that translate four faces of one Fermi surface

onto four faces of the other. Since the average of $\mathbf{Q}_{\pm}$ is $\mathbf{G}/2$, the nesting wave vectors may be written as $\mathbf{Q}_{\pm}=(\mathbf{G}/2)(1\pm\delta)$, where $\delta\approx 0.04$ is a measure of the size difference between the electron and hole Fermi surfaces.

Unlike the condensate of a superconductor, which contains pairs of electrons with zero total momentum, the condensate of an *I* SDW contains pairs of electrons and holes with nonzero total momentum. In the *I* phase of the SDW, the condensate contains two types of electron-hole pairs: one with pair momentum $\mathbf{Q}'_{+}=(\mathbf{G}/2)(1+\delta')$ and the other with pair momentum $\mathbf{Q}'_{-}=(\mathbf{G}/2)(1-\delta')$. Because $0\leqslant\delta'<\delta$, the ordering wave vectors $\mathbf{Q}'_{\pm}$ of the SDW lie closer[26,27] to $\mathbf{G}/2$ than the nesting wave vectors $\mathbf{Q}_{\pm}$. Whereas $\mathbf{Q}_{\pm}$ and δ are fixed by the band-structure topology, $\mathbf{Q}'_{\pm}$ and δ' are solved by minimizing the nesting free energy ΔF and generally depend on temperature. When $\delta'=0$ and $\mathbf{Q}'_{\pm}=\mathbf{G}/2$, the SDW is commensurate. When $\delta'>0$, the *I* SDW has a period of a/δ', corresponding to a node-to-node distance of $1/\delta'$ ML's. For pure Cr just below its Néel temperature,[2] $\delta'\approx 0.037$ and $1/\delta'\approx 27$.

The three sets of possible ordering wave vectors $\mathbf{Q}'_{\pm}$ correspond to the three possible orientations of the nesting wave vectors along the (100), (010), or (001) directions. When pure Cr is cooled below its Néel temperature $T_{\mathrm{N}}\approx 310$ K, six types of domains form.[2] In each domain, the spin polarization $\hat{\mathbf{m}}$ lies along one of two possible directions perpendicular to one of the three sets of wave vectors $\mathbf{Q}'_{\pm}$.

Replacing the strongly peaked Bloch wave functions by delta functions at every lattice site $\mathbf{R}$, the general form for the Cr spin at $\mathbf{R}$ can be simply written as

$$\mathbf{S}(R_z)=\hat{\mathbf{m}}\alpha'_s g(T)\{\cos(\mathbf{Q}'_{+}\cdot\mathbf{R}+\phi_{+})+\cos(\mathbf{Q}'_{-}\cdot\mathbf{R}+\phi_{+})\}$$
$$=(-1)^{2R_z/a}\hat{\mathbf{m}}\alpha_s g(T)\cos[(2\pi/a)\delta' R_z+\theta/2], \quad (1)$$

where α_s and α'_s are constants, $g(T)$ is the temperature-dependent order parameter, and $\theta=\phi_{+}-\phi_{-}$. While θ is arbitrary in the *I* state, $\theta=\pi/2$ (Ref. 28) in the *C* state with $\delta'=0$. Hence, the amplitudes of the *I* and *C* SDW's are given by $\alpha_s g(T)$ and $\alpha_s g(T)/\sqrt{2}$, respectively. Across a second-order *IC* phase transition with the same order parameter g on both sides, the SDW amplitude drops by a factor of $1/\sqrt{2}$ but the rms magnetic moment is continuous. In the *C* phase at low temperatures,[2] the Cr moment is approximately $0.8\mu_B$ and the *C* SDW amplitude $\alpha_s g(0)/\sqrt{2}$ is about 0.4. For pure Cr at low temperatures, $\alpha_s g(0)\approx 0.3$ corresponding to a magnetic moment of $0.6\mu_B$. Both *I* and *C* SDW's are sketched in Fig. 1, where the period of the *I* SDW is somewhat shorter than in pure Cr.

The Coulomb interaction *U* between the electrons and holes on the *a* and *b* Fermi surfaces never explicitly appears in the free energy. It only enters implicitly through the fictitious Néel temperature $T_{\mathrm{N}}^{*}\approx 100$ meV of a perfectly nested alloy with $\delta=0$. For an alloy with $\delta\neq 0$, the actual Néel temperature T_{N} must be less than T_{N}^{*}. In terms of T_{N}^{*}, the free-energy difference between the *P* and SDW phases can be written[26]

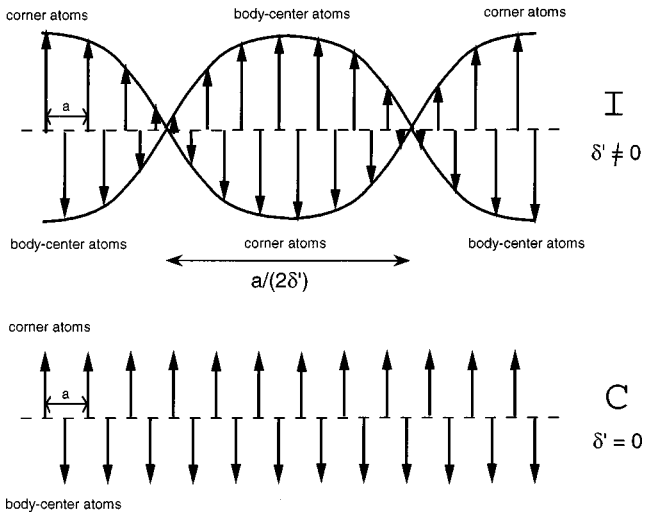

FIG. 1. *I* and *C* SDW's with $\delta'>0$ and $\delta'=0$. For better visualization, the node-to-node distance is substantially shorter than in pure Cr.

$$\Delta F(g,\delta',T,z_0)=\rho_{eh}g^2\ln\left(\frac{T}{T_{\mathrm{N}}^{*}}\right)+\rho_{eh}\sum_{l=0}^{\infty}\left\{g^2\frac{1}{l+1/2}-T\int_{-\infty}^{+\infty}dz\,\ln\left|\frac{D(g,\delta',i\nu_l)}{D(0,\delta',i\nu_l)}\right|\right\}, \quad (2)$$

$$D(g,\delta',i\nu_l)=(i\nu_l-z)[(i\nu_l-z_0/2+z)^2-(z_0\delta'/2\delta)^2]-g^2(2i\nu_l-z_0+2z), \quad (3)$$

where $\nu_l=(2l+1)\pi T$ are the Matsubara frequencies and ρ_{eh} is the density of states of the nested portions of the *a* and *b* Fermi surfaces. When $g=0$, $\Delta F=0$ as expected. The variable of integration in ΔF is $z=v_F(\mathbf{k}\cdot\hat{\mathbf{n}}-k_F)$, where $\hat{\mathbf{n}}$ is normal to one of the octagonal faces of the *a* Fermi surface and v_F (k_F) is the Fermi velocity (momentum).

Doping affects the bulk free energy through the energy mismatch $z_0=4\pi\delta v_F/\sqrt{3}a$ between the *a* and *b* Fermi surfaces. While V impurities increase z_0, Mn impurities lower the mismatch between the Fermi surfaces. When the Mn concentration exceeds about 0.3%, the mismatch is sufficiently small to stabilize the *C* SDW phase with $\delta'=0$ at T_{N}. In units of T_{N}^{*}, the triple point where the *P*, *C*, and *I* phases meet is given by $z_0=4.29T_{\mathrm{N}}^{*}\approx 430$ meV.

Below T_{N}, the electron and hole energies are hybridized by the Coulomb attraction *U*. The resulting quasiparticle energies $\epsilon(z)$ are obtained from the condition $D(g,\delta',\epsilon)=0$. In the *C* state with $\delta'=0$, lower and upper bands are separated by the energy gap $2\Delta\equiv 2\sqrt{2}g$. At low temperatures, 2Δ is about 370 meV. The quasiparticle spectrum of the *I* phase is somewhat more complicated, with two identical energy gaps of roughly 120 meV separated by a third band of quasiparticle states.[29]

The normalization of the free-energy difference ΔF in Eq. (2) is chosen so that for a perfectly nested *C* alloy with $z_0=0$ at $T=0$, $\Delta F(0)=-\rho_{eh}\Delta(0)^2/4$. Since $\rho_{eh}/4$ is the density of states for electrons on the *a* Fermi surface with a

single spin but both spin states are paired, this result is the analogue of the $T=0$ BCS free energy[30] for Cooper pairing.

Due to the lattice mismatch between Cr and Fe, the lattice constant of Cr inside the Fe/Cr/Fe wedge is about 0.6% smaller[5] than in bulk. As discussed in the Introduction, lattice strain has the same qualitative effect as V doping. Therefore, the effects of lattice strain can be modeled by choosing the energy mismatch z_0 to yield the observed periodicity of the SDW. A node-to-node distance of 20 ML at room temperature is obtained with a mismatch of $z_0=6.4T_N^*$, which is substantially larger than the mismatch $z_0\approx 5T_N^*$ in pure Cr.

However, recent work by Marcus *et al.*[6] indicates that lattice strain does not significantly alter the sizes of the Fermi surfaces. Nevertheless, strain does play a crucial role in stabilizing the SDW of pure Cr. We use the energy mismatch to model the effects of lattice strain simply because changes in pressure have qualitatively the same effects as changes in the electron concentration.

III. MODEL I: ANTIFERROMAGNETIC INTERACTIONS AT THE Fe-Cr INTERFACES

Model I assumes that the antiferromagnetic Fe-Cr interactions have the form $A\mathbf{S}_{\rm Fe}^{\rm I,II}\cdot\mathbf{S}(z)$ at interfaces I ($z=a/2$) and II ($z=Na/2$) with coupling constant $A>0$. Such an antiferromagnetic interaction would be expected for microscopically smooth interfaces and is clearly warranted in Fe/Cr wedges. Most measurements on epitaxially grown multilayers[3,10,11] and even some measurements on sputtered multilayers[31] obtain antiferromagnetic interactions at the interfaces. But other measurements on sputtered multilayers[4] suggest that surface roughness interferes with the magnetic coupling between neighboring Fe and Cr layers, at least below T_N. Antiferromagnetic interfacial interactions were confirmed in the first-principles calculations of Mirbt *et al.*[32]

For simplicity, we assume that the Fe moments are either F or AF aligned with $\mathbf{S}_{\rm Fe}^{\rm I}=\mathbf{S}_{\rm Fe}^{\rm II}$ or $\mathbf{S}_{\rm Fe}^{\rm I}=-\mathbf{S}_{\rm Fe}^{\rm II}$, both parallel to the interface. The SDW will then be transversely polarized with respect to the ordering wave vectors along the z axis. While the Fe moments in Fe/Cr wedges satisfy this assumption, the Fe moments in Fe/Cr multilayers may not. The measurements of Schreyer *et al.*[3] on epitaxially grown Fe/Cr multilayers indicate that interfacial steps produce a 90° coupling[13,12] between adjacent Fe moments, which are joined by a helical modulation of the Cr moment. We shall return to this possibility in the final section.

With antiferromagnetic interactions at the interfaces, the free energy of the multilayer or wedge for an interfacial area of a^2 and spacer width $L=(N-1)a/2$ may be written as[16]

$$E=A\{\mathbf{S}_{\rm Fe}^{\rm I}\cdot\mathbf{S}(a/2)+\mathbf{S}_{\rm Fe}^{\rm II}\cdot\mathbf{S}(Na/2)\}+\frac{1}{2}\Delta F a^3(N-1), \quad (4)$$

which assumes that the SDW is rigid with order parameters g and δ' independent of z (but see Ref. 33). Since the interfacial energies always induce some SDW ordering with $g>0$ no matter how high the temperature, the P state is unstable within this model.

In a more realistic, albeit far more complex, model, the SDW amplitude $g(z)$ would vanish inside the spacer above the paramagnetic transition temperature of the multilayer despite some residual ordering near the interfaces at $z=a/2$ and $z=Na/2$. Below the bulk Néel temperature, the SDW amplitude will be enhanced near the interfaces. But the pair coherence length[30] of the I phase $\xi_0\sim\hbar v_F/\pi g$ is about 10 Å, so the SDW order parameters g and δ' are expected to be modified only within 5 or 6 ML from each interface. This has been confirmed by recent first-principles calculations[32] and observed by x-ray magnetic circular dichroism.[31] Even above the bulk Néel temperature of the spacer but below the paramagnetic transition temperature of the multilayer, the equilibrium value of the SDW amplitude (which scales like $1/N$) should be reached within a coherence length or so from the interfaces. Hence, the IC phase boundary evaluated from this model should be qualitatively accurate.

The free energy of an Fe/Cr/Fe trilayer may be obtained in one of two ways. First, the energy E can be evaluated for either ferromagnetically or antiferromagnetically oriented Fe moments. The Fe moments may be fixed in one orientation or the other in an Fe/Cr/Fe trilayer containing permanently magnetized Fe whiskers. Alternatively, we can allow the Fe moment on one side of the trilayer to find its lowest-energy configuration. Of course, this is the case for Fe/Cr wedges, where the thin Fe overlayer is not permanently magnetized. Then the stable magnetic configuration (F or AF) has the lower energy. We shall examine the behavior of Fe/Cr/Fe trilayers from both perspectives in the following discussion.

After fixing the magnetic configurations of the Fe layers, the SDW order parameters g and δ', as well as the arbitrary phase θ,[33] are chosen to minimize the energy E in Eq. (4). The corresponding F and AF energies of the trilayer are

$$E_{\rm F}=-2A\alpha_s g S_{\rm Fe}|\cos\phi|+\frac{1}{2}\Delta F(g,\delta',T)a^3(N-1), \quad (5)$$

$$E_{\rm AF}=-2A\alpha_s g S_{\rm Fe}|\sin\phi|+\frac{1}{2}\Delta F(g,\delta',T)a^3(N-1), \quad (6)$$

where $\phi=(\pi/2)(N-1)(1+\delta')$. The SDW order parameter is restricted to values below the bulk maximum of $g_{max}=1.246T_N^*$, which is achieved in the C SDW phase of a bulk Cr alloy at $T=0$. Note that the number n of SDW nodes inside the Cr spacer is approximately given by $(N-1)\delta'$. For comparison with previous papers, Ref. 16 used the definition $\Lambda=\delta'/\delta$.

Because the nesting free energy ΔF is proportional to $\rho_{eh}T_N^{*2}$, the total free energy E depends only on the dimensionless constant

$$\gamma=\frac{A\alpha_s S_{\rm Fe}}{(V/N)\rho_{eh}T_N^*}, \quad (7)$$

which represents the average coupling strength between Fe and Cr at the interfaces. It can be estimated either from first-principles calculations or by comparison with the experimental data. For example, a value of $\gamma=3$—which will be used later in this section to model the phase diagram of Fe/Cr wedges—corresponds to an average Fe-Cr exchange interaction of 6.8 meV. In bulk Fe, the Fe-Fe interaction is of order 100 meV. So if the Fe-Cr exchange energy at a perfect interface is the same order as the Fe-Fe interaction, then the

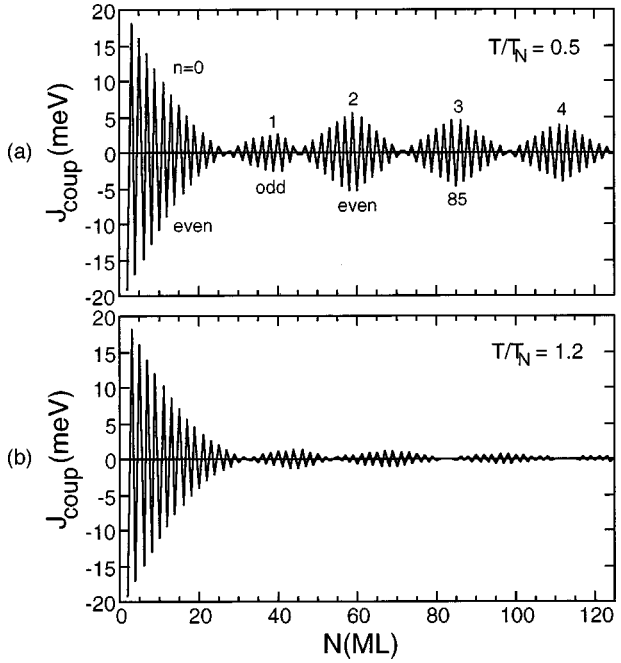

FIG. 2. Model I: Bilinear magnetic coupling in meV as a function of spacer thickness for $z_0/T_N^*=5$, $\gamma=3$, and (a) $T=0.5T_N$ or (b) $T=1.2T_N$.

Fe-Cr interface interaction in Fe/Cr multilayers and wedges is about 1/15 that at a perfect interface. This agrees with recent experiments[34] and with model calculations[35] that the measured Fe-Cr coupling is substantially smaller than expected for a perfect interface. For example, Venus and Heinrich[34] found that the measured coupling is about 1/30 smaller than the coupling given by first-principles calculations[36,24] for a perfect interface. Possible explanations for this suppression are surface roughness and intermixing.

Throughout the remainder of this section and into the next, we shall take the nesting parameter to be $\delta=0.043$ when $z_0/T_N^*=5$. At T_N, this yields a bulk value for the SDW wave vector of $\delta'\approx 0.037$, corresponding to the node-to-node distance of 27 ML observed in pure Cr. For larger values of the energy mismatch in strained Cr, δ is assumed to increase linearly. So $\delta=0.055$ when $z_0/T_N^*=6.4$, which is used to model Fe/Cr wedges. All energies will be scaled by $T_N^*\approx 100$ meV.

Once E_{AF} and E_F are found,[37] the magnetic coupling $J_{coup}=E_{AF}-E_F$ may be evaluated as a function of temperature T and thickness N. Taking $\gamma=3$, $z_0/T_N^*=5$, $(V/N)\rho_{eh}=3.7$ states/Ry atom,[22] and $T=0.5T_N$ or $1.2T_N$, we plot J_{coup} as a function of spacer thickness in Fig. 2. As expected, J_{coup} oscillates between F (>0) and AF (<0) values with a short 2-ML period. Below the Néel temperature, the magnetic coupling decays slowly with the size of the spacer as shown in Fig. 2(a). This behavior is easily understood in terms of the competing energies in Eq. (4). In a large spacer, the wave-vector parameter δ' is more constrained by the bulk free energy $\Delta F(g,\delta')a^3(N-1)/2$. Hence, the SDW cannot deform as easily to maximize the antiferromagnetic Fe-Cr coupling at the interfaces. We prove in Appendix A that J_{coup} falls off like $1/\sqrt{N}$ below T_N.

As shown in Fig. 2(b), the magnetic coupling falls off much more rapidly above the Néel temperature. For large N, Appendix A demonstrates that J_{coup} decreases like $1/N^2$. This behavior was predicted[24] when isolated, extremal points of the Fermi surface are nested but is unexpected for our idealized octahedral Fermi surfaces, where finite regions are nested. Indeed, van Schilfgaarde *et al.*[24] predicted a $1/N^{1.25}$ dependence in this case. Quasiparticle transitions across the necks of the ''electron jack'' or across the hole pockets are believed to be responsible[23] for a magnetic coupling with a $1/N^2$ falloff and a long period of 10–12 ML.[5] A short, 2-ML period coupling with a $1/N^2$ falloff would also result from Ruderman-Kittel-Kasuya-Yosida (RKKY) coupling[24] across a paramagnetic Cr spacer. So above T_N, the RKKY and nesting contributions to the magnetic coupling cannot be distinguished by their dependence on N.

We emphasize that the predicted dependence of J_{coup} on N only holds asymptotically. Pierce *et al.*[38] have found that the short-period coupling of an Fe/Cr multilayer grown at a substrate temperature of 350 °C but measured at room temperature can be fit by a $1/N$ dependence for $N<40$. But as clearly seen in Fig. 2(b), the predicted $1/N^2$ falloff for $T>T_N$ may only be recovered for values of N above 100 or so, particularly when T is not far above the bulk Néel temperature.

For $N<28$, Fig. 2(a) reveals that the magnetic coupling with the lowest free energy is F for odd N and AF for even N. The stable coupling then alternates between F and AF until $N=28$, when a phase slip occurs. For both $N=27$ and $N=28$, the stable coupling is F. Until the next phase slip at $N=46$, the stable coupling is F for even N and AF for odd N. This series of phase slips was observed in the NIST measurements.[5] Each time a phase slip occurs, the number of nodes within the stable SDW increases by one. So the stable SDW is commensurate prior to the first phase slip, contains one node for N between 28 and 45, and two nodes for N between 46 and 71.

Compared to the first-principles predictions of Stoeffler and Gautier,[36] the results of Figs. 2(a) and 2(b) for J_{coup} are about 50% too small. But even when the energy mismatch is enhanced to account for the strain in Fe/Cr multilayers, our results are still roughly 30 times *larger* than the experimentally measured coupling strengths.[39,40] This suggests that the effects of interdiffusion and atomic steps are too complex to be modeled by one or two fitting parameters.

The results of Fig. 2 can be more easily appreciated from the vantage of Fig. 3, which plots the magnetic phase diagram for unstrained ($z_0=5T_N^*$) and strained ($z_0=6.4T_N^*$) Fe/Cr/Fe trilayers with $\gamma=3$. We also display the number n of SDW nodes for the stable magnetic phase as a function of thickness and temperature. The thick solid curves denote the IC transition while the thinner curves denote the transitions between I phases with different n. At a fixed temperature, phase slips occur whenever a solid curve is crossed. Away from a phase slip, the stable magnetic coupling alternates between F and AF with increasing thickness N. On either side of a phase slip, the stable magnetic coupling (AF or F) is the same.

Returning to Figs. 2(a) and 2(b), we find that a phase slip occurs every time a phase boundary in Fig. 3(a) is crossed at $T=0.5T_N$ or $1.2T_N$. At the higher temperature, the phase boundaries are shifted to the right and further apart. For N

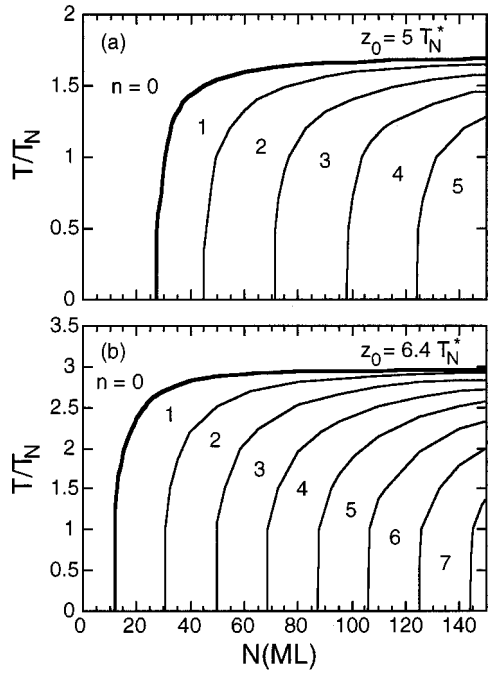

FIG. 3. Model I: Phase diagram of Fe/Cr multilayers and wedges for $\gamma=3$ and (a) $z_0=5T_N^*$ and $T_N=0.384T_N^*$ or (b) $z_0=6.4T_N^*$ and $T_N=0.282T_N^*$. The thick solid curve denotes the *IC* transition while the thin solid curves separate different *I* phases with *n* nodes.

$=45$, the *I* SDW phase with $n=2$ is stable at very low temperatures, but gives way to an *I* SDW phase with $n=1$ between $0.345T_N$ and $1.505T_N$, and finally to a *C* SDW phase with $n=0$ above $1.505T_N$.

If the phase slips occur between thicknesses N_i and N_i-1, then the distance between phase slips shall be denoted by $s_i=N_{i+1}-N_i$. While the SDW is *C* before the first phase slip at N_1, the *I* SDW has $n=i$ nodes for $N_i \leqslant N \leqslant N_{i+1}-1$. The distance s_1 between the first two phase slips is always the smallest. For large Cr spacers, the bulk free energy ΔF dominates the interfacial energies. So below T_N, $s_i \rightarrow 1/\delta'_{\text{bulk}}$ as $i\rightarrow\infty$. In other words, the distance between phase slips approaches the distance between nodes of the bulk SDW. In addition, the distance N_1 to the first phase slip is always less than $1/\delta'_{\text{bulk}}$ and only reaches this value as $\gamma \rightarrow\infty$. Above the bulk Néel temperature and close to the *IC* phase boundary, the phase slip distances s_i become more disparate with the higher s_i's diverging most rapidly as $T \rightarrow T_{IC}$.

For a larger mismatch z_0, the bulk SDW period is smaller so the phase boundaries in Fig. 3(b) are closer together than in Fig. 3(a). At low temperatures, the critical thickness separating the *C* ($n=0$) and *I* ($n=1$) phases shifts downwards as z_0 increases. For both Figs. 3(a) and 3(b), the temperature is normalized by the bulk Néel temperature for that particular energy mismatch. As the mismatch increases, the bulk Néel temperature decreases: $T_N=0.384T_N^*$ when $z_0/T_N^*=5$, while $T_N=0.282T_N^*$ when $z_0/T_N^*=6.4$. In units of T_N^*, the large *N* limits for the *IC* transition temperatures are $0.651T_N^*$ and $0.834T_N^*$ for $z_0/T_N^*=5$ and 6.4, respectively. So paradoxically, the *IC* transition temperature is larger for $z_0=6.4T_N^*$ than for $z_0=5T_N^*$.

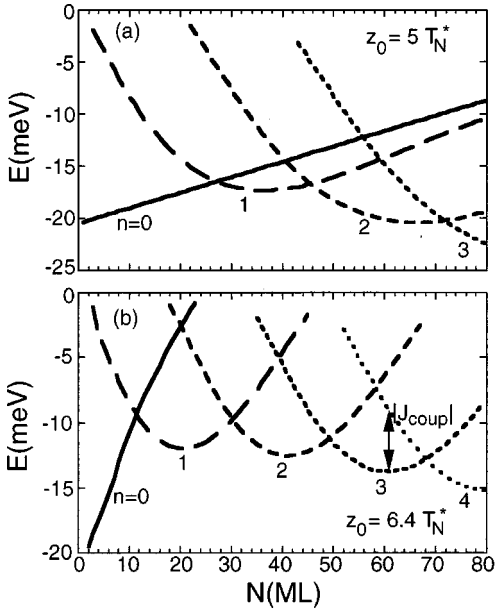

FIG. 4. Model I: Energy in meV versus thickness for an *I* SDW with *n* nodes, with $T/T_N=0.5$ and (a) $z_0=5T_N^*$ or (b) $z_0=6.4T_N^*$.

Fixing $T=0.5T_N$, we plot energy versus *N* for the different SDW solutions in Fig. 4. The region of stability for a SDW with *n* nodes corresponds exactly to the region between the solid curves in Figs. 3(a) and 3(b). Taking the difference between the lowest-energy solution and the one just above it in Fig. 4(a) yields the amplitude of J_{coup} plotted in Fig. 2(a). The *C* SDW solution with $n=0$, drawn as a solid curve, is much more robust for $z_0=5T_N^*$ than for $6.4T_N^*$.

In Fig. 5, we plot the distance s_2 between the second and third phase slips as a function of temperature. Below T_N, s_2 is almost constant and very close to the bulk distance $1/\delta'_{\text{bulk}}$ between SDW nodes. Above T_N, s_2 begins to increase rapidly with temperature. As expected, s_2 diverges as T approaches T_{IC}. This figure bears a striking resemblance to the measured phase slip distance[5] in Fe/Cr wedges. Since the nesting wave vectors do not change with temperature, the

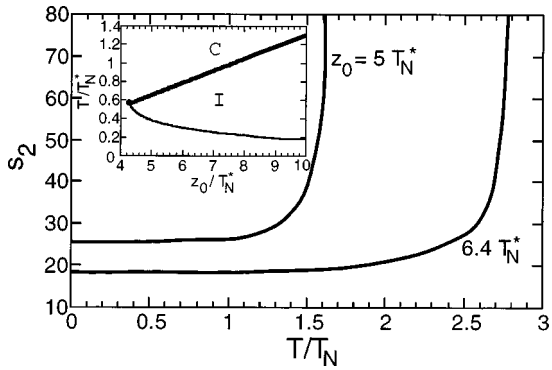

FIG. 5. Model I: Distance s_2 between the second and third phase slips versus temperature for $z_0/T_N^*=5$ and 6.4. Inset is the *IC* transition temperature T_{IC}/T_N^* (thick solid curve) versus energy mismatch z_0/T_N^* for large *N*. Also plotted in the inset is the Néel temperature T_N/T_N^* (thin solid curve) of bulk Cr. The triple point is denoted by a dot.

temperature dependence of s_2 is completely due to the temperature dependence of the bulk SDW free energy.

The dependence of the SDW amplitude and wave vector on thickness was discussed in Refs. 16 and 17. Each time the number of nodes increases by one, the SDW amplitude decreases discontinuously. With increasing N, both g and δ' approach their bulk values and the oscillations about the bulk values become narrower. As N increases between phase slips, the number of SDW nodes remains the same but the SDW stretches to maximize the antiferromagnetic coupling at the interfaces. When n increases by 1, the SDW period suddenly contracts with the addition of another node. We refer the reader to the references above for a more detailed discussion of this behavior.

These results indicate that the C phase is stable for small N or large temperatures. This may be easily understood in terms of the competition between the interface coupling, which maximizes the SDW amplitude at the boundaries, and the intrinsic antiferromagnetism of the spacer, which favors the bulk values of the SDW amplitude and wave vector. While the SDW gains energy $2A\alpha_s S_{\mathrm{Fe}} g|\cos\phi|$ (F) or $2A\alpha_s S_{\mathrm{Fe}} g|\sin\phi|$ (AF) due to the interactions at interfaces, it forfeits energy $[\Delta F(g,\delta') - \Delta F(g_{\mathrm{bulk}},\delta'_{\mathrm{bulk}})]a^3(N-1)/2$ due to the changes in the order parameters of the spacer. When $\delta'=0$, $|\cos\phi|=1$ and $|\sin\phi|=0$ for *odd N*, while $|\cos\phi|=0$ and $|\sin\phi|=1$ for *even N*. Hence, the interactions at the interfaces with F (AF) moments prefer a C (I) SDW in a spacer with odd N and an I (C) SDW in a spacer with even N. If $\Delta F=0$, the interface coupling always favors a C SDW state with $|\cos\phi|$ or $|\sin\phi|$ equal to one.

So for odd N, the C SDW is stabilized with F coupling at a high enough temperature that the bulk free energy $\Delta F(g,\delta'=0)$ is sufficiently small. For even N, the C SDW is favored with AF coupling at a sufficiently high temperature. The same considerations apply for small N: the C SDW is favored with F coupling for odd N and AF coupling for even N.

When N is large, the IC transition temperature is remarkably independent of the Fe-Cr coupling constant γ. In Appendix B, we prove that $T_{IC}(N\to\infty)$ is implicitly given by

$$\sum_{n=0}^{\infty} \mathrm{Re}\left(\frac{1}{X_n^3}\right)=0, \tag{8}$$

where $X_n = n+1/2+iz_0/8\pi T_{IC}(\infty)$. As a consequence, $T_{IC}(\infty)$ depends only on the energy mismatch z_0 and is independent of γ. Both $T_{IC}(\infty)$ and the bulk Néel temperature T_{N} are plotted versus the energy mismatch z_0/T_{N}^* in the inset to Fig. 5. Precisely at the triple point $z_0 \approx 4.29 T_{\mathrm{N}}^*$ where the CI and paramagnetic phase boundaries of bulk Cr meet, $T_{IC}(\infty)=T_{\mathrm{N}}$. With increasing z_0, $T_{IC}(\infty)$ increases but T_{N} decreases. So the IC transition temperature of an Fe/Cr multilayer always exceeds the Néel temperature of bulk Cr. Recall from our previous discussion that lattice strain enhances the effective value for the energy mismatch z_0.

The independence of T_{IC} from γ in the large N limit raises an intriguing question: How is bulk behavior recovered as $\gamma\to 0$? Stabilized by the interfacial coupling energy, a remnant SDW survives above the bulk ordering temperature T_{N}. As N increases, the bulk free energy dominates and g/T_{N}^* falls off like γ/N above T_{N}. Nonetheless, the IC phase boundary for $N\to\infty$ does not depend on γ.[17]

Although $T_{IC}(\infty)$ is independent of γ, the critical thickness $N_1(T=0)$ below which the C SDW is stable at $T=0$ strongly depends on the coupling strength. As shown in Ref. 17 for $z_0/T_{\mathrm{N}}^*=5$, $N_1(0)$ increases from 16 to 53 as γ increases from 1 to 6. For the value of $\gamma=3$ used in Fig. 3(a), $N_1(0)=28$.

IV. MODEL II: SDW NODES AT THE Fe-Cr INTERFACES

Neutron-scattering measurements on multilayers have not followed the same pattern as the NIST measurements on wedges. Although Fig. 3(a) for $z_0=5T_{\mathrm{N}}^*$ predicts an IC transition temperature of about $1.7T_{\mathrm{N}}\approx 530$ K, the I phase is observed to disappear above about 300 K in both epitaxially grown[3] and sputtered[4] Fe/Cr multilayers. As the temperature increases for a fixed N, multilayers do not exhibit the predicted series of I-to-I phase transitions with decreasing numbers of nodes from $n=m$ to $n=m-1$ on up to $n=0$. The different behavior of Fe/Cr wedges and multilayers may be ascribed to the interfacial disorder in multilayers. Noncollinear SDW ordering[13,14] may be produced by the well-separated interfacial steps in epitaxially grown multilayers. Nearby atomic steps in sputtered multilayers may establish SDW nodes near the interfaces,[4] in which case neighboring Fe moments are not magnetically coupled.

If the SDW nodes lie precisely at the Fe-Cr interfaces, then δ' is restricted to the values $\delta'_n=(n-1)/(N-1)$, where $n\geq 2$ is the number of SDW nodes including the two at the interfaces. We evaluate n by minimizing the nesting free energy $\Delta F(g,\delta'_n)$ with respect to both g and n. Like model I, this model also assumes that the SDW is rigid. Hence, the SDW amplitude and wave vector do not depend on the location z inside the spacer.

Because the C SDW does not contain any nodes, the C phase is never stabilized by model II. In Fig. 6(a), the Néel temperature T_{N} and phase boundaries are normalized by the bulk Néel temperature $T_{\mathrm{N,bulk}}$, which is evaluated by allowing δ' to be a continuous parameter. As in the previous section, we take $z_0=5T_{\mathrm{N}}^*$ and $\delta=0.043$. So the bulk value of δ' at $T_{\mathrm{N,bulk}}$ is 0.037, corresponding to a node-to-node distance of 27 ML. These parameters are different than the ones used in Ref. 18. For $T/T_{\mathrm{N,bulk}}=0.2$, the SDW order parameter and wave vector are plotted versus N in Fig. 7.

As N decreases below 41 ML, δ' increases and the SDW period decreases as a half wavelength of the SDW tries to squeeze into the Cr spacer. When $N<27$, δ' is larger than its bulk value so that the SDW period is smaller than in bulk. For $N<20$ ML's, a half wavelength of the SDW cannot squeeze into the Cr spacer without a prohibitive cost in free energy and the Néel temperature vanishes. As N increases, the SDW goes through cycles of expansions followed by sudden contractions with the addition of another node to the SDW. The SDW amplitude and wave vector plotted in Figs. 7(a) and 7(b) are correlated: δ' decreases as g grows larger. In other words, the cyclical expansion and contraction of the SDW follow the same pattern as found for model I in Ref. 16. Only now these cycles also produce a seesaw pattern in T_{N}. The Néel temperature reaches a maximum whenever δ'_n passes near its bulk value of 0.037.

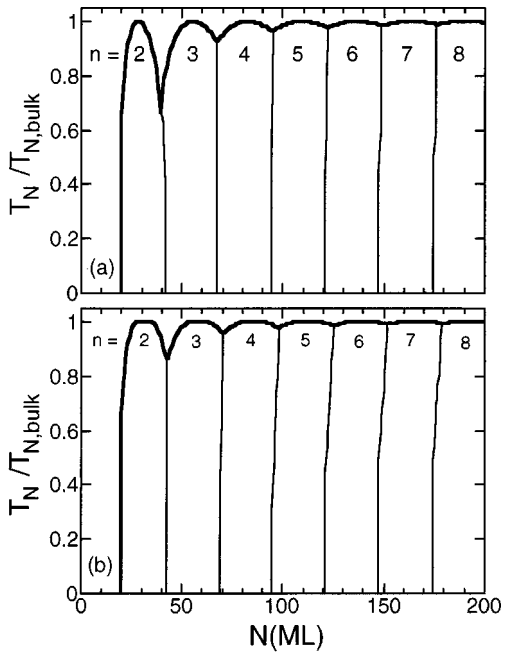

FIG. 6. Model II: Néel temperature (thick solid curve) and phase boundaries (thin solid curve) versus N for $z_0/T_N^*=5$. The number of SDW nodes is given by n. In (a) SDW nodes are fixed at each interface; in (b) the nodes can shift by 3 ML from each interface.

Notice that T_N, g, and δ' all approach their bulk values as $N\rightarrow\infty$. With increasing N, the oscillations about the bulk values become narrower and the seesaw patterns become flatter. For large N, the maxima in T_N are separated by $1/\delta'_{bulk}(T_{N,bulk})\approx 27$ ML.

Unlike the more complex phase diagrams of Fig. 3, Fig. 6(a) only allows a single I-to-I phase transition from $n=m$ to $n=m\pm 1$ before the SDW disappears above T_N. For narrow ranges of thicknesses, phase transitions are allowed between SDW's with different numbers of nodes as a function of temperature. Such a phase transition occurs for $N=122$, when the SDW transforms from $n=6$ to $n=5$ with increasing temperature. As in model I, the SDW amplitude jumps up when n decreases by one.[17] Transition between SDW's with n differing by one in CrMn/Cr multilayers may be easily observed because the neutron-scattering profiles of SDW's with odd and even n are quite different.[4] Very recently, Fullerton and Robertson[15] observed a phase transition from $n=5$ to $n=4$ with increasing temperature in a CrMn/Cr multilayer with $L=200$ Å.

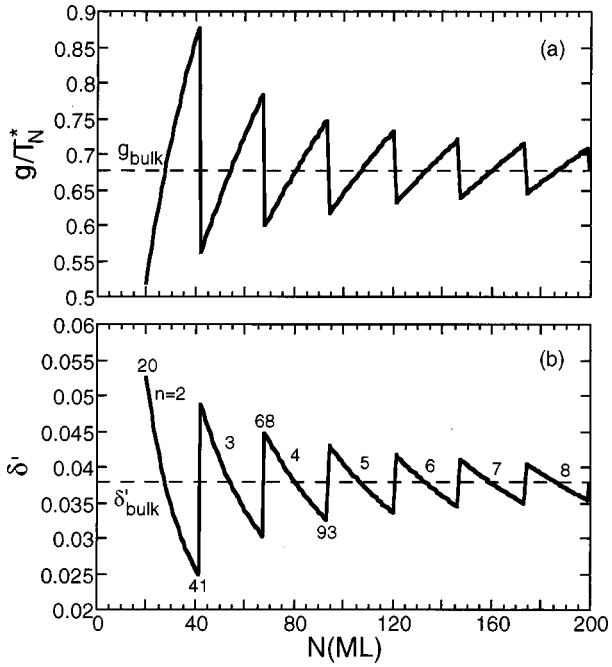

FIG. 7. Model II: (a) SDW order parameter and (b) wave vector versus N for $T/T_{N,bulk}=0.2$ for the same parameters as in Fig. 6, with nodes fixed at each interface. The bulk values are indicated by the dashed lines.

It is clear that forcing the SDW nodes to lie at the Fe-Cr interfaces generates a seesaw pattern in $T_N(N)$, g, and δ'. The shift in δ' along one of the seesaws with fixed n may be difficult to observe due to limitations in experimental resolution (roughly 10%) and the effects of surface roughness, which averages over several values of N. For example, the predicted change in δ' from $N=68$ to 93 at $T/T_{N,bulk}=0.2$ corresponds to a variation in the SDW period from 22 to 31 lattice constants, all with $n=4$. The average SDW period, however, is very close to the bulk value of 27 lattice constants.

For a bulk SDW with $\delta'(T_{N,bulk})\approx 1/27$, Fig. 6(a) predicts that the I phase becomes unstable below 20 ML. But the measured critical thickness[41,4] of 30 ML is much larger. This could be caused by the displacement of the SDW nodes away from the interfaces. Surface roughness may be expected to suppress the SDW ordering within a pair coherence length $\xi_0\approx 5$ ML from the interfaces. If the region within 5 ML from each interface is paramagnetic, then the observed critical thickness of 30 ML would correspond to a ''true'' critical thickness of $30-10=20$ ML, equal to the predicted value. For $N<30$ or temperatures greater than 300 K, the residual antiferromagnetic coupling at the Fe-Cr interfaces may be sufficient to stabilize a C SDW in some regions of the Cr spacer, as found by Fullerton *et al.*[4]

Even if the first 5 ML from the Fe-Cr interface are paramagnetic, however, the Néel temperature would still be expected to contain a deep minimum at 39 + 10 = 49 ML or 74 Å. None has been observed. This sudden drop in the Néel temperature would be softened if the positions of the SDW nodes vary within a few ML from each Fe-Cr interface. For example, imagine that the SDW nodes can shift by 3 ML from each interface. Then for a given spacer thickness N, the SDW amplitude and wave vector would be chosen among seven possible SDW's with lengths N' between N and $N-6$. The SDW with the smallest free energy $\Delta F(N'-1)$ would determine the order parameters of the multilayer. So the SDW would pay a price in condensation energy in order to move its nodes away from the interfaces.

This program was implemented in Fig. 6(b). The first and last SDW nodes lie a minimum distance of $N-6$ ML apart and a maximum distance of N ML apart. As shown, this freedom allows the Néel temperature to linger close to its bulk value. Compared to the Néel temperature of Fig. 6(a), the size of the oscillations about $T_{N,bulk}$ are smaller and the first dip in the Néel temperature is much weaker. The displacement of the SDW nodes from the interfaces is largest

for spacer thicknesses with a depressed Néel temperature when $N'=N$. In addition, the phase boundaries between SDW's with neighboring n are more slanted than in Fig. 6(a).

The measurements by Fullerton *et al.*[4] on sputtered multilayers provide some evidence for this behavior. Fits to their data reveal that the SDW nodes lie very close to the Fe-Cr interfaces *except* for $N=35$, corresponding to a SDW with $n=2$ near the predicted depression in T_N when $N'=N$. For this SDW, Fullerton *et al.* find that the antinodes rather than the nodes lie close to the Fe-Cr interfaces. However, their data for $N=35$ can be equally well described by a SDW with nodes displaced 7 ML from each interface.

V. DISCUSSION AND CONCLUSION

This paper has presented two very different models for the formation of a SDW in an Fe/Cr/Fe trilayer. Within model I, the Fe-Cr interfacial interactions are assumed to be antiferromagnetic. As a result, the SDW antinodes lie near the interfaces. Even above the bulk Néel temperature, the interfacial interaction stabilizes a SDW within the Cr spacer. Surprisingly, this model predicts that the *IC* transition temperature is always larger than the bulk Néel temperature. By contrast, model II assumes that the SDW nodes lie precisely at the Fe-Cr interfaces, although this requirement is somewhat relaxed in Fig. 6(b). As a result, both the Néel temperature and SDW wave vector undergo oscillations with increasing spacer thickness.

Measurements by Unguris *et al.*[5] on Fe/Cr/Fe wedges closely follow the scenario depicted in Fig. 3(b) for model I. In terms of the Néel temperature $T_N=0.384T_N^*\approx 310$ K of unstressed Cr, the *IC* transition of the stressed film is given by $2.1T_N\approx 650$ K. Although the measurements of Ref. 5 only go up to about 550 K, 650 K is just slightly larger than the *IC* transition temperature, which can be extrapolated from the NIST data. Unguris *et al.* observed a very uniform pattern of phase slips with the same s_i depending only on temperature. The values of $\gamma=3$ and $z_0=6.4T_N^*$ used in Fig. 3(b) were chosen to give the smallest possible variation of s_i and a bulk value of $1/\delta'=19$ at $T_N=227$ K, slightly smaller than the observed phase slip distance of 20 ML at 300 K.

For $T=300$ K, the first predicted phase slip at $N_1=13$ ML in Fig. 3(b) occurs earlier than the first observed[5] phase slip at 24 ML in an Fe/Cr/Fe wedge. Accounting for the intermixing of Fe and Cr within the first 5 ML of the wedge,[42] an initial phase slip at $5+19=24$ ML can be obtained using a somewhat larger coupling constant of $\gamma\approx 6$. Intermixing within the first few ML's is also necessary to explain the reversal[5] of the expected F and AF couplings.

Probably due to the restricted temperature range of their measurements and the small size of their wedge ($N<80$ ML), Unguris *et al.* did not observe the phase slip pattern to become nonuniform at high temperatures. Doping the Cr spacer with a small concentration of Mn impurities ($x<0.3\%$) could lower the *IC* transition temperature below 550 K and permit this behavior to be observed.

Some evidence suggests that Fe/Cr multilayers cannot be described by either model. The disappearance of the *I* phase above about 300 K (Refs. 3 and 41) rules out model I, which predicts T_{IC} to be substantially larger than T_N. In disagreement with model II, the observed Néel temperature[41,4] $T_N(N)$ of sputtered Fe/Cr multilayers shows no sign of the dips and peaks associated with the cyclical expansion and contraction of the SDW.

On the other hand, model II correctly predicts that the SDW may undergo a transition from $n=m$ to $n=m-1$ nodes with increasing temperature before entering the paramagnetic state. This behavior, which was recently observed in CrMn/Cr multilayers,[15] is quite different than the series of phase transitions from $n=m$ to $n=m-1$ to $n=m-2$ and on up to $n=0$ predicted by model I. A refined version of model II, which no longer ties the SDW nodes to the interfaces, produces a smoother Néel temperature $T_N(N)$ and may explain most properties of sputtered multilayers.

But even such a refined model cannot stabilize the *H* SDW observed by Schreyer *et al.*[3] in epitaxially grown multilayers. For small thicknesses and low temperatures, a *H* SDW is believed to couple adjacent Fe moments at a 90° angle. The Fe moment returns to its original orientation every other Fe layer.[12] Since a *H* SDW does not occur in bulk Cr, it must be stabilized by the interfacial energy. In the presence of well-separated interfacial steps, a *H* SDW is found to have a lower free energy above T_N than either the *I* SDW predicted by model I or the *P* phase predicted by model II.[14]

To summarize, we have evaluated the phase diagram of Fe/Cr trilayers using two different methods. While model I assumes that the magnetic interactions at the Fe-Cr interfaces are antiferromagnetic, model II assumes that the SDW nodes lie at the interfaces. The results of model I are in good agreement with measurements on Fe/Cr wedges, where interfacial disorder is minimized. Sputtered multilayers may be adequately described by a refined version of model II, which allows the SDW nodes to shift away from the interfaces with some cost in condensation energy. However, neither model satisfactorily describes the properties of epitaxially-grown Fe/Cr multilayers.

We would like to thank Dr. Eric Fullerton, Dr. Daniel Pierce, Dr. Lee Robertson, Professor Andreas Schreyer, and Dr. Mark Stiles for helpful discussions. This research was supported by Oak Ridge National Laboratory managed by Lockheed Martin Energy Research Corp. for the U.S. Department of Energy under Contract No. DE-AC05-96OR22464.

APPENDIX A: BEHAVIOR OF J_{coup}

This appendix uses model I to evaluate the behavior of $J_{coup}=E_{AF}-E_F$ for large N. For notational convenience, we set $\rho_{eh}T_N^*=1$ and $T_N^*=1$ so that both g and ΔF are dimensionless. Minimizing the AF and F energies of Eqs. (5) and (6) with respect to g and δ', we find

$$-2\gamma|\cos\phi|+\frac{\partial\Delta F(g,\delta',T)}{\partial g}(N-1)=0 \quad \text{(F)}, \quad \text{(A1)}$$

$$-2\gamma|\sin\phi|+\frac{\partial\Delta F(g,\delta',T)}{\partial g}(N-1)=0 \quad \text{(AF)}, \quad \text{(A2)}$$

$$\gamma g\pi \sin\phi \,\mathrm{sgn}(\cos\phi)+\frac{\partial \Delta F(g,\delta',T)}{\partial \delta'}=0 \quad \text{(F)}, \tag{A3}$$

$$-\gamma g\pi \cos\phi \,\mathrm{sgn}(\sin\phi)+\frac{\partial \Delta F(g,\delta',T)}{\partial \delta'}=0 \quad \text{(AF)}, \tag{A4}$$

where $\phi=\pi(N-1)(1+\delta')/2$.

As $N\to\infty$, both g and δ' approach their bulk values. To first order in $\Delta g=g-g_{\rm bulk}$ and $\Delta\delta'=\delta'-\delta'_{\rm bulk}$, the above relations become

$$-2\gamma|\cos\phi|+(N-1)\{F_{11}\Delta g+F_{12}\Delta\delta'\}=0 \quad \text{(F)}, \tag{A5}$$

$$-2\gamma|\sin\phi|+(N-1)\{F_{11}\Delta g+F_{12}\Delta\delta'\}=0 \quad \text{(AF)}, \tag{A6}$$

$$\pi g_{\rm bulk}\sin\phi \,\mathrm{sgn}(\cos\phi)+F_{12}\Delta g+F_{22}\Delta\delta'=0 \quad \text{(F)}, \tag{A7}$$

$$-\pi g_{\rm bulk}\cos\phi \,\mathrm{sgn}(\sin\phi)+F_{12}\Delta g+F_{22}\Delta\delta'=0 \quad \text{(AF)}, \tag{A8}$$

where $F_{11}=\partial^2\Delta F/\partial g^2$, $F_{12}=\partial^2\Delta F/\partial g\,\partial\delta'$, and $F_{22}=\partial^2\Delta F/\partial\delta'^2$ are evaluated at $g_{\rm bulk}$ and $\delta'_{\rm bulk}$. For large N, a very small change in the SDW wave vector is required to optimize the interfacial coupling with $|\cos\phi|\to1$ (F) and $|\sin\phi|\to1$ (AF). So $\sin\phi\to0$ and $\cos\phi\to0$ in these two cases.

To obtain the behavior of $J_{\rm coup}$ as $N\to\infty$, we examine the coupling near a local maximum in $J_{\rm coup}(N)$, roughly midway between phase slips. We assume that the stable coupling is AF with n SDW nodes and that the unstable coupling is F with $n-1$ nodes. For example, the thickness $N=85$ in Fig. 2 satisfies this condition with $n=3$. Consequently, the wave vectors of the SDW's can be written

$$\delta'_{\rm F}=\frac{n-1}{N-1}+\frac{\eta_{\rm F}}{N^x}, \tag{A9}$$

$$\delta'_{\rm AF}=\frac{n}{N-1}+\frac{\eta_{\rm AF}}{N^y}, \tag{A10}$$

where $1<x<y$ below $T_{\rm N}$. Since the AF coupling is assumed to be stable, n is odd when N is odd and even when N is even. So as expected, $|\cos\phi|\approx1$ for F coupling and $|\sin\phi|\approx1$ for AF coupling.

For large N, it is easy to show that

$$|\cos\phi|\approx1+\frac{\eta_{\rm F}^2}{N^{2(x-1)}}\frac{\pi^2}{8} \quad \text{(F)}, \tag{A11}$$

$$|\sin\phi|\approx1+\frac{\eta_{\rm AF}^2}{N^{2(y-1)}}\frac{\pi^2}{8} \quad \text{(AF)}, \tag{A12}$$

$$\sin\phi \,\mathrm{sgn}(\cos\phi)\approx\frac{\eta_{\rm F}}{N^{x-1}}\frac{\pi}{2} \quad \text{(F)}, \tag{A13}$$

$$\cos\phi \,\mathrm{sgn}(\sin\phi)\approx\frac{\eta_{\rm AF}}{N^{y-1}}\frac{\pi}{2} \quad \text{(AF)}. \tag{A14}$$

Then using Eqs. (A5)–(A8) and assuming $x\leqslant2$, we find $\Delta g_{\rm AF}\sim1/N$, $\Delta\delta'_{\rm AF}\sim1/N$, $\Delta g_{\rm F}\sim1/N^{x-1}$, and $\Delta\delta'_{\rm F}\sim1/N^{x-1}$ with $y=2$. So long as $x<2$, the leading order term in $J_{\rm coup}$ is given by

$$J_{\rm coup}\approx2\gamma\Delta g_{\rm F}\sim\frac{1}{N^{x-1}}. \tag{A15}$$

It only remains to evaluate the exponent x.

Near the envelope maximum, the unstable F energy with N ML's and $n-1$ nodes is nearly equal to the unstable F energy with $N+2$ ML and $n+1$ nodes. Expanding Eq. (5) in powers of $\Delta g_{\rm F}$, $\Delta\delta'_{\rm F}$, and $\eta_{\rm F}/N^{x-1}$, we obtain

$$\begin{aligned}
&-2\gamma(g_{\rm bulk}+\Delta g_{\rm F}^{(N)})[1+\eta_{\rm F}^2\pi^2/(8N^{2(x-1)})]+\Delta F_{\rm bulk}(N-1)\\
&\quad+\left\{\frac{1}{2}F_{11}\Delta g_{\rm F}^{(N)2}+F_{12}\Delta g_{\rm F}^{(N)}\Delta\delta'^{(N)}_{\rm F}+\frac{1}{2}F_{22}\Delta\delta'^{(N)2}_{\rm F}\right\}\\
&\quad\times(N-1)\\
&=-2\gamma(g_{\rm bulk}+\Delta g_{\rm F}^{(N+2)})\\
&\quad\times(1+\eta_F^2\pi^2/[8(N+2)^{2(x-1)}])+\Delta F_{\rm bulk}(N+1)\\
&\quad+\left\{\frac{1}{2}F_{11}\Delta g_{\rm F}^{(N+2)2}+F_{12}\Delta g_{\rm F}^{(N+2)}\Delta\delta'^{(N+2)}_{\rm F}\right.\\
&\quad\left.+\frac{1}{2}F_{22}\Delta\delta'^{(N+2)2}_{\rm F}\right\}(N+1),
\end{aligned} \tag{A16}$$

where $\Delta F_{\rm bulk}$ is the bulk free energy evaluated at $g_{\rm bulk}$ and $\delta'_{\rm bulk}$. Since $\Delta g_{\rm F}^{(N)}\sim\Delta\delta'^{(N)}_{\rm F}$, we conclude that $\Delta g_{\rm F}^{(N)2}\sim\Delta F_{\rm bulk}/N$. So below $T_{\rm N}$, $x=3/2$ and $J_{\rm coup}\sim1/\sqrt{N}$.

Above $T_{\rm N}$, $\Delta F_{\rm bulk}=0$ and $g_{\rm bulk}=0$. Then Eq. (A16) can be used to show that $\Delta g_{\rm F}\sim1/N$ with $x=y=2$. To order $1/N$, the F and AF order parameters are identical with

$$\Delta g_{\rm AF}=\Delta g_{\rm F}=\frac{2\gamma}{N}\frac{F_{22}}{F_{11}F_{22}-F_{12}^2}, \tag{A17}$$

$$\Delta\delta'_{\rm AF}=\Delta\delta'_{\rm F}=\frac{2\gamma}{N}\frac{F_{12}}{F_{11}F_{22}-F_{12}^2}. \tag{A18}$$

Therefore, $J_{\rm coup}$ vanishes to order $1/N$ and its leading-order behavior is given by $J_{\rm coup}\sim1/N^2$.

APPENDIX B: DERIVATION OF T_{IC}

At the IC phase boundary of model I, a C SDW with $n=0$ and order parameter g_0 has the same free energy as an I SDW with $n=1$ and order parameters g_1 and δ'_1. As $N\to\infty$, g_0, g_1, and δ'_1 all tend to zero. Therefore, the free energy $\Delta F(g,\delta')$ may be expanded in powers of g and $u\equiv z_0\delta'/8\pi T\delta$:

$$\Delta F(g,\delta')\approx g^2(\ln\ T-S_1+u^2S_3)+\frac{1}{8\pi^2T^2}g^4S_3, \tag{B1}$$

where

$$S_1=\sum_{n=0}^{\infty}\mathrm{Re}\left(\frac{1}{X_n}-\frac{1}{n+1/2}\right), \tag{B2}$$

$$S_{2m+1\geqslant 3}=\sum_{n=0}^{\infty}\mathrm{Re}\left(\frac{1}{X_n^{2m+1}}\right), \tag{B3}$$

$$X_n=n+\frac{1}{2}+i\frac{z_0}{8\pi T}. \tag{B4}$$

If N is even, then the stable C phase above T_{IC} is AF while the stable I phase below T_{IC} is F. Their energies are

$$\frac{2}{a^3}E_{\mathrm{AF}}=\Delta F(g_0,0)-\frac{2\gamma}{N-1}g_0, \tag{B5}$$

$$\frac{2}{a^3}E_{\mathrm{F}}=\Delta F(g_1,\delta_1')-\frac{2\gamma}{N-1}g_1|\cos\phi_1|, \tag{B6}$$

where $\phi_1=\pi(N-1)(1+\delta_1')/2$.

The minimization conditions for E_{F} and E_{AF} with respect to g and δ' are given by

$$g_0(\ln T-S_1)+\frac{1}{2\pi^2T^2}S_3g_0^3=\frac{\gamma}{N-1}, \tag{B7}$$

$$g_1(\ln T-S_1+u_1^2S_3)+\frac{1}{2\pi^2T^2}S_3g_1^3=\frac{\gamma}{N-1}|\cos\phi_1|, \tag{B8}$$

$$-\pi\gamma\delta^2\sin\phi_1\,\mathrm{sgn}(\cos\phi_1)=2g_1\left(\frac{z_0}{8\pi T}\right)^2\delta_1'\{S_3-2u_1^2S_5\}-\frac{1}{\pi^2T^2}g_1^3\left(\frac{z_0}{8\pi T}\right)^2\delta_1'S_5. \tag{B9}$$

The last relation implies that

$$\delta_1'\approx\frac{1}{N-1}+\eta S_3\frac{1}{(N-1)^3}+\cdots, \tag{B10}$$

which agrees with Eq. (A9) when $x=3$ and the ferromagnetically coupled SDW has $n-1=1$ node. Hence, $\sin\phi_1\sim S_3/N^2$ and $|\cos\phi_1|-1\sim S_3^2/N^4$.

Using Eqs. (B7) and (B8), it is simple to show that

$$(g_1-g_0)(\ln T-S_1)=-u_1^2S_3g_1-\frac{1}{2\pi^2T^2}S_3(g_1^3-g_0^3). \tag{B11}$$

Consequently, g_1-g_0 is of order S_3/N^3. But to order $1/N^4$, the equality $E_{\mathrm{F}}=E_{\mathrm{AF}}$ requires

$$\frac{2\gamma}{N-1}(g_1-g_0)=(g_1^2-g_0^2)(\ln T-S_1)+u_1^2S_3g_1^2. \tag{B12}$$

Substituting Eqs. (B7) and (B8), we conclude that g_1-g_0 is also of order $1/N^4$. So S_3 must be of order $1/N$ and vanish as $N\to\infty$. Therefore, the condition for the IC transition temperature in the limit of large N is given by Eq. (8), independent of γ.

[1] M. N. Baibich, J. M. Broto, A. Fert, F. Nguyen Van Dau, F. Petroff, P. Eitenne, G. Creuzet, A. Friederich, and J. Chazelas, Phys. Rev. Lett. **61**, 2472 (1988).

[2] E. Fawcett, Rev. Mod. Phys. **60**, 209 (1988); E. Fawcett, H. L. Alberts, V. Yu. Galkin, D. R. Noakes, and J. V. Yakhmi, *ibid.* **66**, 25 (1994).

[3] A. Schreyer, J. F. Ankner, Th. Zeidler, H. Zabel, C. F. Majkrzak, M. Schäfer, and P. Grünberg, Europhys. Lett. **32**, 595 (1995); A. Schreyer, C. F. Majkrzak, Th. Zeidler, T. Schmitte, P. Bödeker, K. Theis-Bröhl, A. Abromeit, J. A. Dura, and T. Watanabe, Phys. Rev. Lett. **79**, 4914 (1997).

[4] E. E. Fullerton, S. D. Bader, and J. L. Robertson, Phys. Rev. Lett. **77**, 1382 (1996).

[5] J. Unguris, R. J. Celotta, and D. T. Pierce, Phys. Rev. Lett. **67**, 140 (1991); **69**, 1125 (1992).

[6] P. M. Marcus, S.-L. Qiu, and V. L. Moruzzi, J. Phys.: Condens. Matter **29**, 6541 (1998).

[7] T. M. Rice, A. Jayaraman, and D. B. McWhan, J. Phys. Colloq. **32**, C1 39 (1971).

[8] R. Griessen and E. Fawcett, Physica B & C **91B**, 205 (1977).

[9] J. Mattson, B. Brumitt, M. B. Brodsky, and J. B. Ketterson, J. Appl. Phys. **67**, 4889 (1990).

[10] T. G. Walker, A. W. Pang, H. Hopster, and S. F. Alvarado, Phys. Rev. Lett. **69**, 1121 (1992).

[11] C. Turtur and G. Bayreuther, Phys. Rev. Lett. **72**, 1557 (1994).

[12] S. Adenwalla, G. P. Felcher, E. E. Fullerton, and S. D. Bader, Phys. Rev. B **53**, 2474 (1996).

[13] J. C. Slonczewski, Phys. Rev. Lett. **67**, 3172 (1991); J. Magn. Magn. Mater. **150**, 13 (1995).

[14] R. S. Fishman, Phys. Rev. Lett. **81**, 4979 (1998).

[15] E. E. Fullerton and J. L. Robertson (private communication).

[16] Z. P. Shi and R. S. Fishman, Phys. Rev. Lett. **78**, 1351 (1997).

[17] R. S. Fishman and Z. P. Shi, J. Phys.: Condens. Matter **10**, L277 (1998).

[18] R. S. Fishman, Phys. Rev. B **57**, 10 284 (1998).

[19] A. W. Overhauser, Phys. Rev. Lett. **4**, 226 (1960); Phys. Rev. **128**, 1437 (1962).

[20] W. M. Lomer, Proc. Phys. Soc. London **80**, 489 (1962).

[21] P. A. Fedders and P. C. Martin, Phys. Rev. **143**, 8245 (1966).

[22] S. Asano and J. Yamashita, J. Phys. Soc. Jpn. **23**, 714 (1967).

[23] M. D. Stiles, Phys. Rev. B **48**, 7238 (1993); **54**, 14 679 (1996).

[24] M. van Schilfgaarde and F. Herman, Phys. Rev. Lett. **71**, 1923 (1993); M. van Schilfgaarde, F. Herman, S. S. P. Parkin, and J. Kudrnovský, *ibid.* **74**, 4063 (1995).

[25] D. Li, J. Pearson, S. D. Bader, E. Vescovo, D.-J. Huang, P. D. Johnson, and B. Heinrich, Phys. Rev. Lett. **78**, 1154 (1997).

[26] R. S. Fishman and S. H. Liu, Phys. Rev. B **48**, 3820 (1993).

[27] R. S. Fishman, X. W. Jiang, and S. H. Liu, Phys. Rev. B **58**, 414 (1998).

[28] X. W. Jiang and R. S. Fishman, J. Phys.: Condens. Matter **9**, 3417 (1997).

[29] R. S. Fishman and V. S. Viswanath, Phys. Rev. B **55**, 8347 (1997).

[30] See, for example, A. Fetter and J. Walecka, *Quantum Theory of Many-Particle Systems* (McGraw Hill, New York, 1971), pp. 426 and 451.

[31] M. A. Tomaz, W. J. Antel, Jr., W. L. O'Brien, and G. R. Harp, Phys. Rev. B **55**, 3716 (1997).

[32] S. Mirbt, A. M. N. Niklasson, B. Johannson, and H. L. Skriver, Phys. Rev. B **54**, 6382 (1996).

[33] In the *C* phase of bulk Cr alloys, charge conservation requires that $\theta=\pi/2$, which also guarantees that the rms moment is continuous across a second-order *IC* phase boundary. Because θ is now chosen to minimize the interfacial coupling energy in both the *I* and *C* phases, we have implicitly assumed that the SDW amplitudes rather than the rms moments are equal near the Cr-Fe interface in *I* and *C* phases with the same order parameter *g*. For the *C* phase, charge conservation (Ref. 28) then requires that between 0.005 and 0.014 electrons per Cr atom are transferred from the Fe layers to the Cr spacer within a coherence length ξ_0 from the interface.

[34] D. Venus and B. Heinrich, Phys. Rev. B **53**, R1733 (1996).

[35] M. Freyss, D. Stoeffler, and H. Dreyssé, Phys. Rev. B **56**, 6047 (1997).

[36] D. Stoeffler and F. Gautier, Phys. Rev. B **44**, 10 389 (1991).

[37] In Refs. 14 and 16, all energies were normalized by the dimensionless density of states $(V/N)\rho_{eh}T_{\mathrm{N}}^{*}\approx 0.0272$ in order to simplify the notation.

[38] D. T. Pierce, J. A. Stroscio, J. Unguris, and R. J. Celotta, Phys. Rev. B **49**, 14 564 (1994).

[39] P. Grünberg, S. Demokritov, A. Fuss, M. Vohl, and J. A. Wolf, J. Appl. Phys. **69**, 4789 (1991).

[40] M. From, L. X. Liao, J. F. Cochran, and B. Heinrich, J. Appl. Phys. **75**, 6181 (1994).

[41] E. E. Fullerton, J. E. Mattson, C. H. Sowers, and S. D. Bader, Scr. Metall. Mater. **33**, 1637 (1995).

[42] A. Davies, J. A. Stroscio, D. T. Pierce, and R. J. Celotta, Phys. Rev. Lett. **76**, 4175 (1996).